

# Infrared absorption nano-spectroscopy using sample photoexpansion induced by tunable quantum cascade lasers

Feng Lu and Mikhail A. Belkin\*

Department of Electrical and Computer Engineering, The University of Texas at Austin, Austin, Texas 78758, USA  
\*mbelkin@ece.utexas.edu

**Abstract:** We report a simple technique that allows obtaining mid-infrared absorption spectra with nanoscale spatial resolution under low-power illumination from tunable quantum cascade lasers. Light absorption is detected by measuring associated sample thermal expansion with an atomic force microscope. To detect minute thermal expansion we tune the repetition frequency of laser pulses in resonance with the mechanical frequency of the atomic force microscope cantilever. Spatial resolution of better than 50 nm is experimentally demonstrated.

©2011 Optical Society of America

**OCIS codes:** (300.6430) Spectroscopy, photothermal; (300.6340) Spectroscopy, infrared; (170.5810) Scanning microscopy; (140.5965) Semiconductor lasers, quantum cascade; (310.6628) Subwavelength structures, nanostructures.

---

## References and Links

1. B. H. Stuart, *Infrared Spectroscopy: Fundamentals and Applications* (Wiley, New York, 2004).
2. I. W. Levin and R. Bhargava, "Fourier transform infrared vibrational spectroscopic imaging: integrating microscopy and molecular recognition," *Annu. Rev. Phys. Chem.* **56**(1), 429–474 (2005), and references therein.
3. M. Born and E. Wolf, *Principles of Optics*, 6th ed. (Pergamon, Oxford, 1987).
4. M. Troccoli, L. Diehl, D. P. Bour, S. W. Corzine, N. Yu, C. Y. Wang, M. A. Belkin, G. Hofler, R. Lewicki, G. Wysocki, F. K. Tittel, and F. Capasso, "High performance quantum cascade lasers grown by metal-organic vapor phase epitaxy and their applications to trace gas sensing," *J. Lightwave Technol.* **26**(21), 3534–3555 (2008).
5. B. Knoll and F. Keilmann, "Near-field probing of vibrational absorption for chemical microscopy," *Nature* **399**(6732), 134–137 (1999).
6. F. Huth, M. Schnell, J. Wittborn, N. Ocelic, and R. Hillenbrand, "Infrared-spectroscopic nanoimaging with a thermal source," *Nat. Mater.* **10**(5), 352–356 (2011).
7. T. Taubner, R. Hillenbrand, and F. Keilmann, "Performance of visible and mid-infrared scattering-type near-field optical microscopes," *J. Microsc.* **210**(3), 311–314 (2003).
8. M. B. Raschke, L. Molina, T. Elsaesser, D. H. Kim, W. Knoll, and K. Hinrichs, "Apertureless near-field vibrational imaging of block-copolymer nanostructures with ultrahigh spatial resolution," *ChemPhysChem* **6**(10), 2197–2203 (2005).
9. A. J. Huber, A. Ziegler, T. Köck, and R. Hillenbrand, "Infrared nanoscopy of strained semiconductors," *Nat. Nanotechnol.* **4**(3), 153–157 (2009).
10. A. Dazzi, R. Prazeres, F. Glotin, and J. M. Ortega, "Local infrared microspectroscopy with subwavelength spatial resolution with an atomic force microscope tip used as a photothermal sensor," *Opt. Lett.* **30**(18), 2388–2390 (2005).
11. A. Dazzi, R. Prazeres, F. Glotin, J. M. Ortega, M. Al-Sawaftah, and M. de Frutos, "Chemical mapping of the distribution of viruses into infected bacteria with a photothermal method," *Ultramicroscopy* **108**(7), 635–641 (2008).
12. K. Kjoller, J. R. Felts, D. Cook, C. B. Prater, and W. P. King, "High-sensitivity nanometer-scale infrared spectroscopy using a contact mode microcantilever with an internal resonator paddle," *Nanotechnology* **21**(18), 185705 (2010).
13. C. Prater, K. Kjoller, and R. Shetty, "Nanoscale infrared spectroscopy," *Mater. Today* **13**(11), 56–60 (2010).
14. We obtain sample temperature change in the range 5–50 K using the experimental parameters reported in Refs. [10,12,13] and the simulation results reported in Ref. [11].
15. A. A. Kosterev, Y. A. Bakirkin, R. F. Curl, and F. K. Tittel, "Quartz-enhanced photoacoustic spectroscopy," *Opt. Lett.* **27**(21), 1902–1904 (2002).
16. H. Hida, M. Shikida, K. Fukuzawa, S. Murakami, K. Sato, K. Asaumi, Y. Iriye, and K. Sato, "Fabrication of a quartz tuning-fork probe with a sharp tip for AFM systems," *Sens. Actuators A Phys.* **148**(1), 311–318 (2008).

17. G. Y. Chen, R. J. Warmack, T. Thundat, D. P. Allison, and A. Huang, "Resonance response of scanning force microscopy cantilevers," *Rev. Sci. Instrum.* **65**(8), 2532–2537 (1994).
18. A. Dazzi, F. Glotin, and R. Carminati, "Theory of infrared nanospectroscopy by photothermal induced resonance," *J. Appl. Phys.* **107**(12), 124519 (2010).
19. J. R. Taylor, *Classical Mechanics* (University Science Books, Herndon, VA, 2005).
20. U. Rabe, K. Janser, and W. Arnold, "Vibrations of free and surface-coupled atomic force microscope cantilevers: theory and experiment," *Rev. Sci. Instrum.* **67**(9), 3281–3293 (1996).
21. N. Bloembergen, "Pulsed laser interactions with condensed matter," *Mat. Res. Soc. Symp. Proc.* **51**, 3 (1985).
22. J. E. Mark, ed., *Physical Properties of Polymers Handbook*, 2nd ed. (Springer, New York, 2007).
23. T. Sikanen, T. Zwinger, S. Tuomikoski, S. Franssila, R. Lehtiniemi, C.-M. Fager, T. Kotiaho, and A. Pursula, "Temperature modeling and measurement of an electrokinetic separation chip," *Microfluidics Nanofluidics* **5**(4), 479–491 (2008).
24. R. Martini, C. Gmachl, J. Falciglia, F. G. Curti, C. G. Bethea, F. Capasso, E. A. Whittaker, R. Paiella, A. Tredicucci, A. L. Hutchinson, D. L. Sivco, and A. Y. Cho, "High-speed modulation and free-space optical audio/video transmission using quantum cascade lasers," *Electron. Lett.* **37**(3), 191–193 (2001).
25. C. Y. Wang, L. Kuznetsova, V. M. Gkortsas, L. Diehl, F. X. Kärtner, M. A. Belkin, A. Belyanin, X. Li, D. Ham, H. Schneider, P. Grant, C. Y. Song, S. Haffouz, Z. R. Wasilewski, H. C. Liu, and F. Capasso, "Mode-locked pulses from mid-infrared quantum cascade lasers," *Opt. Express* **17**(15), 12929–12943 (2009).
26. A. Hugi, R. Terazzi, Y. Bonetti, A. Wittmann, M. Fischer, M. Beck, J. Faist, and E. Gini, "External cavity quantum cascade laser tunable from 7.6 to 11.4  $\mu\text{m}$ ," *Appl. Phys. Lett.* **95**(6), 061103 (2009).
27. A. W. M. Lee, B. S. Williams, S. Kumar, Q. Hu, and J. L. Reno, "Tunable terahertz quantum cascade lasers with external gratings," *Opt. Lett.* **35**(7), 910–912 (2010).

## 1. Introduction

Mid-infrared (mid-IR) absorption spectroscopy in the "molecular fingerprint" region ( $\lambda = 2.5\text{--}15\ \mu\text{m}$ ) is a powerful and ubiquitous technique for in situ analysis of chemical and biomedical samples [1]. Because of the diffraction limit [2], traditional mid-IR imaging techniques, such as Fourier-transform infrared (FTIR) microscopy [3], cannot image or take sample spectra on nanoscale. Here we present a technique of mid-IR nano-imaging and spectroscopy of thin-film samples with better than 50 nm spatial resolution using tunable quantum cascade lasers (QCLs) [4] and a standard atomic force microscope (AFM).

Currently, mid-IR scattering-type near-field scanning optical microscopy (s-NSOM) [5] is the most common technique for mid-IR imaging of samples on nanoscale. This technique produces sample images in mid-IR with spatial resolutions of  $\lambda/100$  or better by detecting light scattered by a sharp metal tip on top of a sample [5–9]. However, all s-NSOM methods require sophisticated homodyne- or heterodyne-based optical setups [5–9] to detect small optical signal produced by tip scattering and distinguish it from the background scattering produced by sample, tip shaft, etc. This makes it difficult to operate s-NSOM setups outside of optics laboratories. In addition the sample spectra produced by s-NSOM mostly originate from spectral variation of the real part of the sample dielectric constant [5–9] and have different bandshapes compared to the mid-IR absorption spectra of the same compound. This makes sample chemical identification more difficult, since mid-IR absorption spectra cannot be directly compared with s-NSOM spectra.

A mid-IR nanoscale imaging technique in which light absorption is detected by measuring associated local thermal expansion in samples by an AFM cantilever has been reported recently [10–13]. The AFM deflection signal there is directly proportional to sample absorption. The spatial resolution of this method is determined by the thermal diffusing length in sample during the laser pulse, which is below 100 nm in typical chem/bio polymers excited with sub-100 ns light pulses. This approach (which works at any wavelength and is referred to as "*photoexpansion microscopy*" here) results in a very simple experimental setup only requires a pulsed light source and a standard AFM. However, the photoexpansion microscopy techniques in Refs. [10–13], required high-fluence optical pulses to produce detectable photoexpansion signal. In particular, pulse fluencies of about  $0.1\ \text{J}/\text{cm}^2$  from free-electron lasers [10,11] or optical parametric oscillators [12,13] were used. Not only that high-fluence pulse requirement results in bulky optical sources, but 5–50 K of temperature change [14] will likely lead to sample damage, especially for biological samples.

We report a technique that allows performing photoexpansion microscopy using orders of magnitude lower energy optical pulses that can be produced by compact light sources such as

tunable QCLs. Our approach is based on moving the repetition frequency of laser pulses in resonance with the mechanical frequency ( $\nu_0$ ) of an AFM cantilever bending mode. We illuminate sample with low-energy light pulses at repetition frequencies in resonance with  $\nu_0$  (typically in the range 10 kHz-1 MHz). The AFM cantilever then “integrates” contributions from many of light pulses. We note that this approach is conceptually similar to quartz-enhanced photoacoustic spectroscopy that is used for gas sensing [15]. The AFM response is enhanced by a Q-factor of the cantilever which may be over  $5 \times 10^3$  in air [16] and above  $10^5$  in vacuum [17]. Details of the cantilever-sample interaction in photoexpansion microscopy are shown in Fig. 1(a). The AFM is operated in contact mode. Sample photoexpansion happens on a time scale much shorter than the mechanical response time of the AFM cantilever ( $>5 \mu\text{s}$ , assuming cantilever resonant frequency  $<200 \text{ kHz}$ ). As a result, force  $F_T$  (see Fig. 1(a)) acts on the cantilever during sample photoexpansion and pushes the cantilever up to produce initial cantilever deflection  $\Delta z_I$  [18]. The cantilever is then undergoing linear oscillations around its equilibrium position  $z_0$  (see Fig. 1(a)) [10,12,13,18]. Small amplitude motion of the AFM cantilever in contact mode can be represented by a simple harmonic oscillator equation:

$$\ddot{z} + 2\gamma\dot{z} + \omega_0^2(z - z_0)^2 = F_T(t), \quad (1)$$

where  $\omega_0 = 2\pi\nu_0$  is the radial eigenfrequency of the bending mode of the AFM cantilever in contact with sample and  $\gamma$  is the damping factor for the cantilever oscillations. If the force  $F_T$  is applied at a repetition frequency that coincides with  $\nu_0$  we expect to see a resonant enhancement of the AFM response as [19]

$$\Delta z \approx \Delta z_I \times Q, \quad (2)$$

where  $\Delta z$  is the cantilever deflection in case of resonant enhancement,  $\Delta z_I$  is the deflection induced by a single light pulse on a sample (such as that used in Refs. [10–13].), and  $Q = \omega_0/2\gamma$  is the quality factor of the cantilever oscillation.

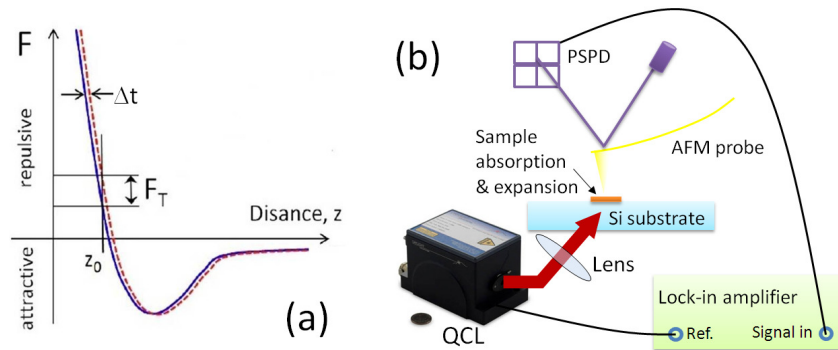


Fig. 1. (a) Mechanism of AFM cantilever deflection during sample photoexpansion. Blue solid curve shows the dependence of the interaction force between the sample surface and the AFM cantilever tip on tip-surface distance ( $z$ ), assuming sample surface is at  $z = 0$ . Red dashed curve is shifted along  $z$ -axis by sample photoexpansion  $\Delta t$ .  $F_T$  is the photoexpansion force acting on the AFM cantilever;  $z_0$  is the position of the AFM cantilever in contact mode. The figure is not drawn to scale. (b) Schematic of experimental setup for photoexpansion microscopy in mid-IR as described in text. A photograph of an actual QCL source used in experiments is shown in comparison with a US 25¢ coin to indicate device dimensions.

## 2. Resonant enhancement of photoexpansion signal and photoexpansion spectra

We used tunable mid-IR QCLs for proof-of-principle demonstration of our method. Figure 1(b) shows our experimental setup. QCLs are electrically-pumped semiconductor lasers [4]; their pulse length and pulse repetition frequency are easily controlled by an electric power supply. QCLs are highly compact and require no external cooling in pulsed operation. In our case, the lasers were operated with 40 ns light pulses and provided approximately 100 mW of

peak power (pulse energy of 4 nJ) on sample surface; the pulse repetition frequency could be tuned between 10 and 250 kHz. Thin-film polymer samples were deposited on undoped silicon substrates that were transparent in mid-IR. Samples were illuminated through the bottom of the substrate; the laser light was focused to  $\approx 100$   $\mu\text{m}$  radius spot. The cantilever deflection signal (“A-B” signal from the AFM position sensitive photodetector) was fed into a lock-in amplifier referenced by a QCL trigger signal. Figure 2(a) shows the dependence of the lock-in output (referred to as “the photoexpansion signal” below) on the repetition frequency of laser pulses. Our AFM cantilever had the first bending mode eigenfrequency of approximately 10 kHz with a Q-factor of  $\approx 50$  in air and the second bending mode eigenfrequency of approximately 60 kHz with a Q-factor of  $\approx 100$  in air. In contact with sample, these two resonances are shifted to higher frequencies [20]. Experimentally, we varied the laser pulse repetition frequency and recorded the value of the photoexpansion signal from a film of SU-8 polymer. The results are shown in Fig. 2(a). Two resonant peaks are clearly visible and they correspond to the first two cantilever bending modes. Approximately 100 times enhancement in the photoexpansion signal is observed as the repetition frequency of the QCL pulses was tuned to coincide with the second resonant frequency of approximately 155 kHz, see Fig. 2(a).

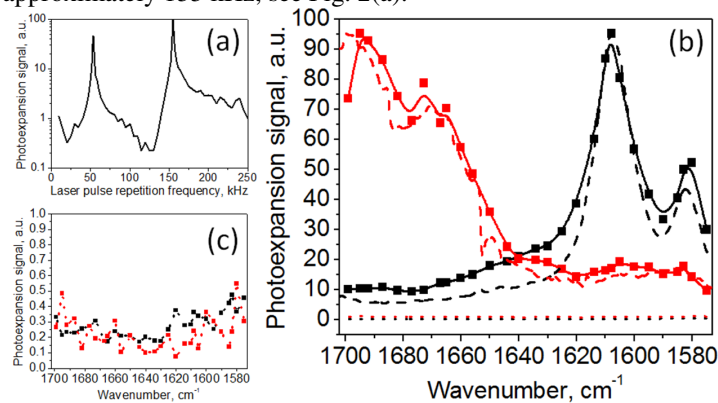


Fig. 2. (a) The photoexpansion signal recorded as a function of the QCL pulse repetition frequency. (b) Photoexpansion spectra. Square data points and solid lines are the photoexpansion spectra of SU-8 (black) and LOR-3A (red) obtained with the laser repetition frequency set at the AFM cantilever resonance of 155 kHz (solid lines are B-splines connecting the data points). Dashed lines are the absorption spectra of SU-8 (black) and LOR-3A (red) as measured by a FTIR spectrometer. Dotted lines near zero-level are the photoexpansion spectra of SU-8 (black) and LOR-3A (red) obtained with the laser repetition frequency set at 130 kHz, away from the AFM cantilever resonance. (c) Zoom-in of the photoexpansion spectra obtained with the laser pulse repetition frequency set at 130 kHz (dotted lines in (b)). Squares are the data points. The spectral features are indistinguishable from noise.

To verify that the enhanced signal in Fig. 2(a) is useful for spectroscopy, we set the repetition frequency of QCL pulses at the high-frequency resonance in Fig. 2(a), tuned the emission wavelengths, and recorded the photoexpansion signal as a function of wavelength to produce “photoexpansion spectra”. The results are presented in Fig. 2(b) for 300-nm-thick SU-8 and LOR-3A polymer films. The data is normalized to the QCL power output at different wavelengths. The photoexpansion spectra are in nearly perfect agreement with mid-IR absorption spectra of the polymers obtained with FTIR as shown in Fig. 2(b). To demonstrate the importance of resonant signal enhancement, we tuned the repetition frequency of QCL pulses to 130 kHz, away from the AFM cantilever mechanical resonance and attempted to record the photoexpansion spectra of the same samples; in this case the spectral features were indistinguishable from noise, see Figs. 2(b,c).

### 3. Simulations and experimental demonstration of high spatial resolution

The spatial resolution of photoexpansion microscopy is principally determined by thermal diffusion length in sample during laser pulse,  $l_D$  [10–13,18]. We may estimate it as  $l_D \sim$

$(k\tau/\rho C)^{1/2}$ , where  $k$ ,  $\rho$ , and  $C$  are the thermal conductance, volume density, heat capacity of a sample, respectively, and  $\tau$  is the duration of the laser pulse [21]. Using typical values of  $\kappa \approx 0.5 \text{ W m}^{-1} \text{ K}^{-1}$  and  $\rho C \approx 2 \text{ J cm}^{-3} \text{ K}^{-1}$  of chem/bio polymers [22], we expect to have  $l_D \approx 100 \text{ nm}$  for excitations with 40 ns pulses. This simple estimate is supported by a more accurate picture provided by simulation results presented in Fig. 3. Two types of inhomogeneous samples are simulated with an absorbing compound either positioned on top of (Figs. 3(a,b)) or embedded within (Figs. 3(c,d)) a non-absorbing compound. The data demonstrates high ( $\sim 50 \text{ nm}$ ) spatial resolution of the technique and shows that sample heating is limited to 10 mK in our experiments. The sample cools down within a few microseconds, before the next QCL pulse arrives.

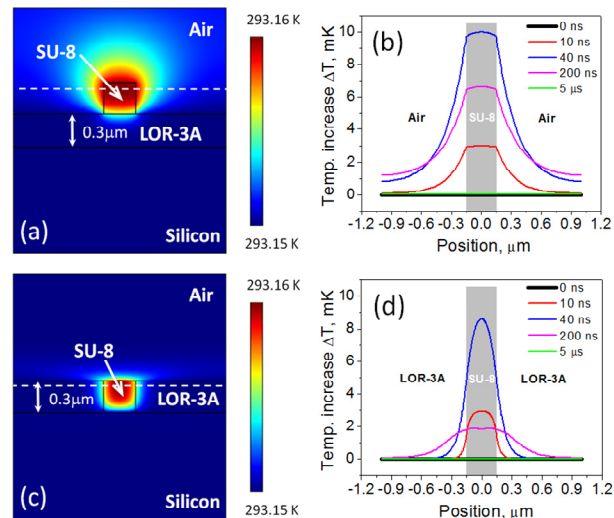


Fig. 3. Simulations of the temperature distribution in inhomogeneous polymer samples before, during, and after a single laser pulse. The samples are assumed to be illuminated by a 100 mW 40 ns-square pulse, focused to a 100  $\mu\text{m}$ -radius area. (a) Temperature distribution at the end of a laser pulse in a sample consisting of a SU-8 block (300 nm wide and 300 nm thick) placed on top of a 300-nm-thick layer of LOR-3A on a silicon substrate. (b) Temperature variation along the dashed line in (a) before (0 ns), during (10 ns), and after (40 ns, 200 ns, and 5  $\mu\text{s}$ ) the laser pulse. (c) Temperature distribution at the very end of a laser pulse in a sample consisting of a SU-8 block (300 nm wide and 300 nm thick) embedded within a 300-nm-thick layer of LOR-3A on a silicon substrate. (d) Temperature variation along the dashed line in (c) before (0 ns), during (10 ns), and after (40 ns, 200 ns, and 5  $\mu\text{s}$ ) the laser pulse. The SU-8 parameters are taken from Ref. [23]: thermal conductance  $\kappa = 0.3 \text{ W m}^{-1} \text{ K}^{-1}$ , material density  $\rho = 1.2 \times 10^3 \text{ kg m}^{-3}$  and heat capacity  $C = 1.2 \times 10^3 \text{ J kg}^{-1} \text{ K}^{-1}$ ;  $\kappa$ ,  $\rho$ , and  $C$  for LOR-3A are assumed to be the same for simplicity. The power absorption coefficient is set as  $1.7 \times 10^3 \text{ cm}^{-1}$  for SU-8, according to the FTIR data at  $1180 \text{ cm}^{-1}$ . For figure clarity, LOR-3A is assumed non-absorbing.

To experimentally demonstrate high spatial resolution, we prepared a sample composed of an image of a Texas Longhorn made of a 50-nm-thick layer of SU-8 polymer deposited on a silicon substrate coated with a 70-nm-thick film made of LOR-0.7A polymer. Sample AFM topographic image is displayed in Fig. 4(a). We have measured a series of photoexpansion spectra at four points, each separated by a distance of 50 nm from its neighbor as shown in the inset to Fig. 4(a). A tunable QCL source operating in the range  $1140\text{--}1205 \text{ cm}^{-1}$  was used to obtain these spectra. The photoexpansion spectra are shown in Figs. 4(b–e), along with the FTIR spectra of SU-8 and LOR-0.7A polymers. The spectra demonstrate that we can clearly distinguish the chemical composition of the SU-8-made Longhorn and the LOR-0.7A background with better than  $\lambda/170$  spatial resolution. The data also proves that our technique is capable of measuring spectra from extremely thin (50-nm-thick) samples and is able to identify chemical compounds. Finally, Fig. 4(f) shows the “photoexpansion infrared image” of the sample obtained by fixing the laser frequency at  $1204 \text{ cm}^{-1}$  and recording the

photoexpansion signal during the AFM scan. As seen in Figs. 4(b-e), LOR-0.7A polymer produces considerably stronger photoexpansion signal than the SU-8 pattern. As a result, the SU-8 pattern appears dark in Fig. 4(f).

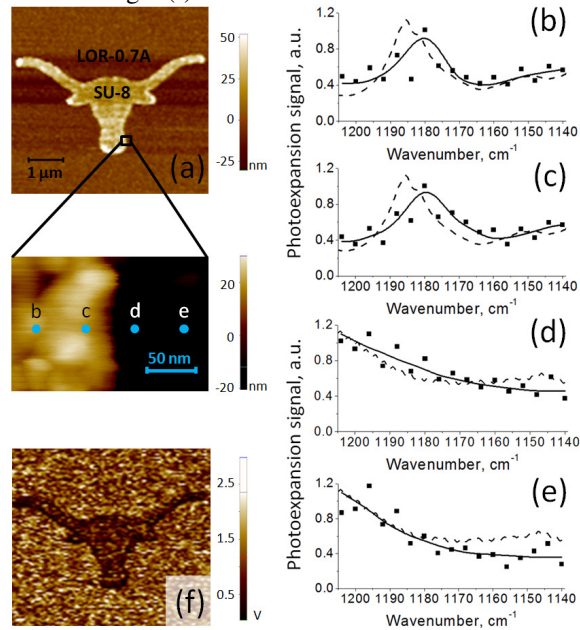


Fig. 4. (a) The AFM topographic image of the 50-nm-thick SU-8 pattern of a Texas Longhorn on top of a 70-nm-thick LOR-0.7A film on an undoped silicon substrate. Inset: the zoom-in image of the section of the SU-8 pattern with four points marking the positions at which the photoexpansion spectra shown in (b-e) are taken. The separation between the adjacent points is 50 nm. (b-e) Photoexpansion spectra (squares are data points, solid lines are for eye guiding) obtained at four sample points shown in (a). Dashed lines are FTIR absorption spectra of SU-8 (b,c) and LOR-0.7A (d,e). (f) Photoexpansion image of Texas Longhorn pattern in (a) taken at laser wavelength of  $1204\text{ cm}^{-1}$ . The image size is 128 by 128 pixels, each pixel correspond to a 50-nm-by-50-nm square.

#### 4. Conclusion

We demonstrated a technique that allows performing absorption spectroscopy on nanoscale using low-power light sources such as mid-IR QCLs. Experimental setup is extremely simple to implement and operate. Sample heating is limited to 10 mK. Spatial resolution of  $\lambda/170$  is experimentally demonstrated and may be further improved using shorter QCL pulses. We note that, with proper driver electronics, QCLs can produce sub-nanosecond pulses [24] and mode-locked QCLs have recently been demonstrated to provide a train of picosecond pulses [25]. Tunable QCLs with considerably broader tuning range and higher output power than those used in our experiments are also available [26]. Our method can be readily extended for nanoscale imaging and spectroscopy in THz spectral range using THz QCLs [27] and spatial resolution better than  $\lambda/1000$  is expected for THz photoexpansion microscopy. We also expect that the sensitivity of our technique will be further increased by 1-2 orders of magnitude using AFM cantilevers with higher quality factors.

#### Acknowledgments

The authors acknowledge the financial support from the Robert A. Welch Foundation grant No. F-1705. Sample fabrication was carried out in the Microelectronics Research Center at the University of Texas at Austin, which is a member of the National Nanotechnology Infrastructure Network. The authors are thankful to Daylight Solutions, Inc. for providing demo-versions of tunable QCL systems for these experiments.